Plasma in-liquid method for reduction of zinc oxide in zinc nanoparticle synthesis

2015 Mater. Res. Express 2 025004

(http://iopscience.iop.org/2053-1591/2/2/025004)

Materials Research Express

RECEIVED
17 September 2014

ACCEPTED FOR PUBLICATION
22 December 2014

PUBLISHED
21 January 2015

PAPER

Plasma in-liquid method for reduction of zinc oxide in zinc nanoparticle synthesis

Novriany Amaliyah[1,2], **Shinobu Mukasa**[1], **Shinfuku Nomura**[1], **Hiromichi Toyota**[1] **and Tomohide Kitamae**[1]

[1] Graduate School of Science and Engineering, Ehime University, Matsuyama 790-8577, Japan
[2] Department of Mechanical Engineering, Hasanuddin University, Makassar 90245, Indonesia

E-mail: amaliyah_nophie@yahoo.com

Keywords: nanoparticles, microwave plasma, liquid, reduction

Abstract

Metal air-batteries with high-energy density are expected to be increasingly applied in electric vehicles. This will require a method of recycling air batteries, and reduction of metal oxide by generating plasma in liquid has been proposed as a possible method. Microwave-induced plasma is generated in ethanol as a reducing agent in which zinc oxide is dispersed. Analysis by energy-dispersive x-ray spectrometry (EDS) and x-ray diffraction (XRD) reveals the reduction of zinc oxide. According to images by transmission electron microscopy (TEM), cubic and hexagonal metallic zinc particles are formed in sizes of 30 to 200 nm. Additionally, spherical fiber flocculates approximately 180 nm in diameter are present.

1. Introduction

Metal-air batteries have attracted excitement recently due to their wide application in electric vehicles, next-generation electronics, as well for energy storage. Lithium, aluminum, iron, and zinc show great promise for use in air batteries. Among these kinds of metals, zinc, particularly as nanoparticles, has attracted great interest due to its low equivalent weight, abundance, and high-energy density [1]. Moreover, it is also safe and environmentally friendly [2–5]. However, in the zinc air battery, a combination of high-energy density of metal anodes with atmospheric oxygen can lead to the formation of zinc oxide in large quantities [6–8].

Several morphologies of zinc, such as zinc nanoparticle [9, 10], zinc nanowire [11], zinc nanofiber [12], zinc nanotube [13] and zinc nanosheets [14] were synthesized by various methods, including in-liquid plasma from zinc wire, laser ablation from zinc metal, electromagnetic levitation gas condensation from zinc, shortcut hydrothermal strategy synthesis from zinc acetate, electron cyclotron resonance (ECR) plasma from zinc metal, ball-milling process from ZnO and amorphous boron, mechanical deformation process using hexagonal Zn oxide powder, simple thermal vapor phase deposition from zinc powder, metalorganic chemical vapor deposition from $Zn(C_2H_5)_2$ and thermochemical reduction from zinc sulfide (ZnS) powder.

Zinc oxide nanomaterial synthesis by zinc oxidation has been reported in numerous studies [15–21], but little research has been conducted into its reduction. It is necessary to balance zinc production with zinc recycling. The recycling of zinc is a critical and beneficial supplement to its primary metal production. Additionally, zinc plays an essential role in preventing from decreasing energy use, minimizing emissions as well as reducing waste materials [22].

When microwave or radio-frequency-induced plasma is generated at the surface of a metallic electrode submerged into a liquid, nanoparticles are synthesized by erosion of the electrode. In-liquid plasma has been successful in the synthesis of many kinds of nanoparticles such as zinc, zinc oxide, tungsten oxide, silver, gold, and magnesium hydroxide to name a few [23, 24]. By applying plasma to a zinc electrode in ethanol, metallic zinc nanoparticles are produced, while, in water, a mixture of zinc and zinc oxide nanoparticles is formed. This suggests that the oxidative or reductive atmosphere of the vapor of the liquid determined the physical properties of the synthesized nanoparticles. Plasma can be observed easily in the vapor, which was generated by the evaporation of the surrounding liquid.

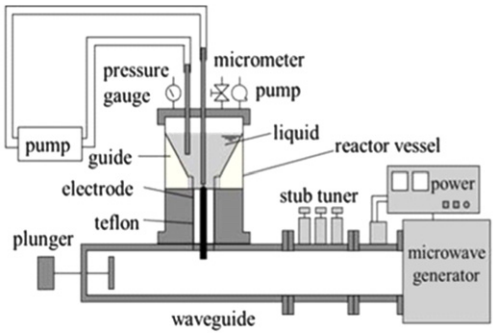

Figure 1. Experimental Apparatus.

The objective of this research is to reduce ZnO powder by microwave-induced plasma in ethanol, with the ethanol being the reducing agent. The synthesized materials were identified using an absorption spectrophotometer, energy-dispersive x-ray spectrometry (EDS) and x-ray diffraction (XRD) (M21X, Mac Science), and as well as observed using a transmission electron microscope (TEM) (JEM-2100, JEOL).

2. Experimental method

The apparatus used in this experiment is shown in figure 1. The reaction vessel is a transparent polycarbonate tube with an inner diameter of 55 mm and outer diameter of 60 mm. A coaxial electrode consisting of an inner conductor of a sharpened copper rod 5 mm in diameter, dielectric Teflon, and outer conductor of brass, was placed perpendicular to the bottom of the vessel. The bottom of the vessel was tapered at an angle of 60 degrees to feed the ZnO powder efficiently to the top of the electrode where the plasma was generated. A copper tube 3 mm in outer diameter and 2 mm in inner diameter used as a counter electrode was placed 2 mm away from the coaxial electrode.

ZnO powder, labeled 200 mesh, 99.999% (NEWMET KOCH) was used. Two different concentrations were applied. For high density dispersion, 3.0 g, 5.0 g, and 6.0 g of ZnO powder were dissolved in 80 ml ethanol, respectively. For low density dispersion, 0.1 g, 0.2 g, and 0.3 g of ZnO powder were used. It was initially stirred manually and then applied to an ultrasonic device until the powder was dispersed sufficiently. The dispersion was poured into the vessel and the pressure in the vessel was decreased to 30 kPa using an aspirator. The liquid was circulated using a gear pump, and funneled from the counter electrode toward the top of the inner electrode.

A 2.45 GHz microwave in TE10 mode passed through a rectangular waveguide, was converted within TEM mode and then subsequently passed through the coaxial electrode. By adjusting a plunger and stab tuner, the input power was increased until plasma ignition occurs between the coaxial electrode and counter electrode. After plasma ignition, the plasma was maintained at 235 W. The period of the plasma generation lasted ten minutes for low density dispersion, and eight and a half minutes for high density liquid dispersion. A different time of plasma generation was caused by liquid densities. When using a high density dispersion, the ZnO powder after a few minutes of plasma irradiation covers the tip of electrode and makes it difficult for continous plasma generation to occur. With low density dispersion, the plasma remains stable until irradiation has continued for 10 min, because there is no ZnO powder covering the tip of the electrode.

3. Result and discussion

During plasma generation, the purple color of plasma emission was observed by naked eye, and the emission spectrum was measured using a spectroscope (PMA-11, HAMAMATSU). Characteristic Zn lines were detected at 468.0, 472.2, 481.1 and 636.2 nm, and the excitation temperature was approximately 3400 K as estimated from emission intensity of these lines by the Boltzmann plot method. Among the three different amounts of ZnO powder (0.1, 0.2, and 0.3 g), the dispersion of 0.2 g was chosen to be the representative result for low density because at this dispersion, plasma was very stable and continuously presented a purple color, which is recognized as the color of zinc.

Figure 2(a) shows the absorption spectroscopy of the 0.2 g dispersion as a function of time, from 0 min (before plasma generation) to 2, 4, 6, 8, and 10 min (after plasma generation) as taken by a spectrophotometer (UV-1800, Shimadzu). During plasma generation, there is a great reduction as the absorbance decreases. It can be seen near 360 nm and 380 nm wavelengths. A wide gap of ZnO between 320 and 390 nm has been reported

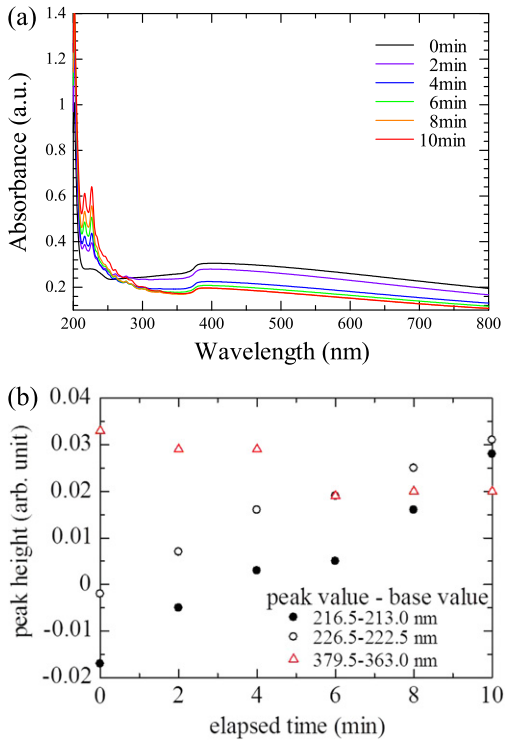

Figure 2. (a) Absorption spectroscopy. (b) The peak height for elapsed time of plasma generation.

for other techniques [25–28]. The other peak observed around 200 to 250 nm on the short-wavelength side is believed to be the result of the formation of zinc nanoparticles. Syntheses of zinc nanoparticles from a zinc rod by plasma in liquid showed the same peak around 220 nm [24]. Research into nanoparticle synthesis by laser ablation has reported that a sharp peak for Zn nanoparticles appears at 232.4 nm [29] and similarly, it has reported around 230 nm for synthesis by radiation chemical reduction [30]. Since a peak for carbon has also been reported to appear around 230 nm, one of the peaks might be derived from Zn and another from carbon, however, this has not been clarified yet.

Figure 2(b) shows peak height of the absorbance, which was obtained by subtracting the base of the peak from the peak value. On the short-wavelength side where a Zn peak is assumed to have been obtained, the peak height increased during the elapsed time of plasma generation. While on the long-wavelength side where a ZnO peak was observed, the peak height decreased. The Beer–Lambert law predicts that the intensity of an absorption peak is directly proportional with the concentration of the compound.

After plasma generation in the dispersion of 0.2 g ZnO in 80 ml of ethanol, the product adhered to the tip of the coaxial electrode is shown in figure 3(a) and residue after evaporation of liquid is shown in figure 3(b). The TEM images of the particles are shown in figure 4. ZnO nanoparticles before plasma generation were a mixture of rectangular and hexagonal crystals of 50 to 200 nm in length and rods approximately 200 nm in length, as shown in figure 4(a). TEM images of particles collected from the tip of the electrode, and from the residue after evaporation of liquid are shown in figures 4(b) and (c), respectively. Good crystallinity of cubic particle about 30–200 nm in diameter is found from the tip of the electrode. It has been reported that zinc nanoparticles in cubic shape have been synthesized by plasma in liquid method using zinc wire [24]. Another rectangular particle is observed in the residue of liquid after evaporation. Although the particles seemed to be in crystalline form and similar to ZnO particles before plasma generation, the amount of oxygen after plasma generation was negligible according to the EDS spectrum in figures 5(a) and (b). This EDS spectra was conducted for a nanoparticle collected at the tip of electrode, for which the TEM image shows a different shape from the ZnO TEM image before plasma irradiation. The mass ratio of oxygen to zinc was found to be 6% which was smaller than the theoretical value of ZnO which was approximately 24%.

There were no significant differences of particle synthesized when using 0,1 and 0.3 g of ZnO powder.

For high density dispersion, plasma generation at a dispersion of 6.0 g ZnO in 80 ml ethanol was relatively more stable than the dispersions of 3.0 g and 5.0 g of ZnO powder, even though the nanoparticles synthesized showed no significant difference in shape or size.

After plasma generation, TEM images of particle were found to show two types of particles, white polygonal ones and spherical fiber-flocculated ones, as shown in figure 6(a). The diameter of the spherical particles was

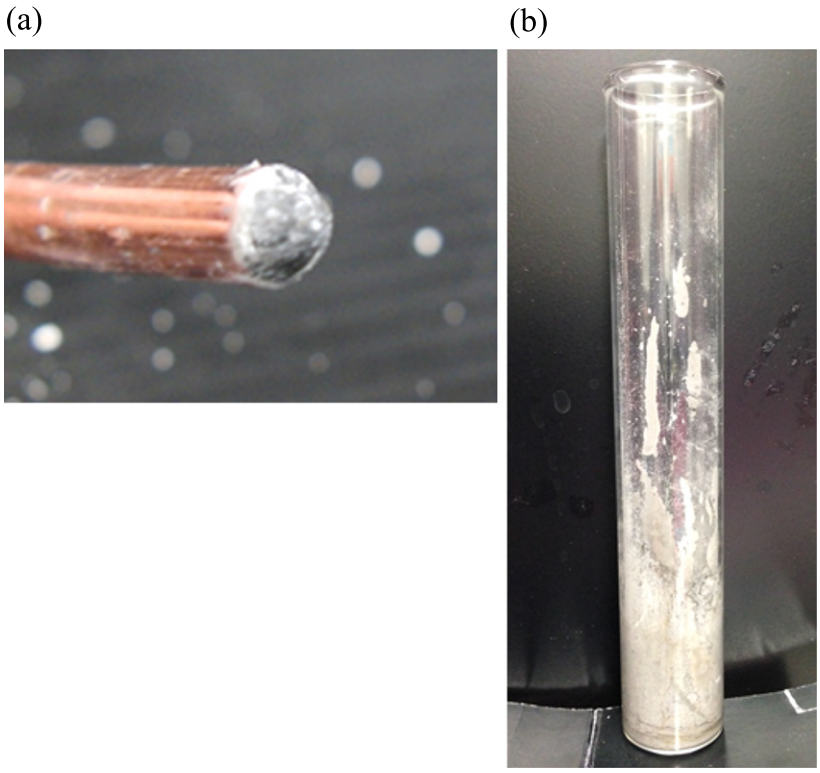

Figure 3. (a) Product adhering to the tip of the electrode, (b) residue after liquid evaporation.

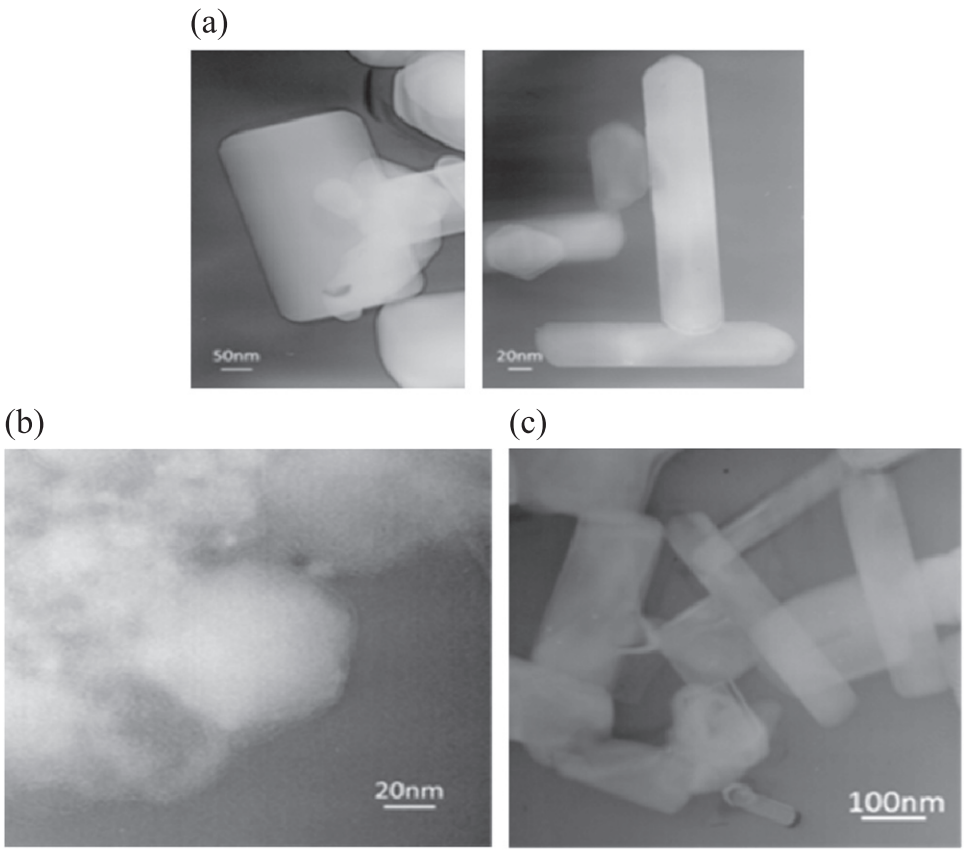

Figure 4. (a) TEM image of ZnO before plasma irradiation. (b) TEM images of nanoparticles in the dispersion of 0.2 gm in 80 ml ethanol, particles collected from the tip of electrode. (c) TEM image of particles from residue after liquid evaporation.

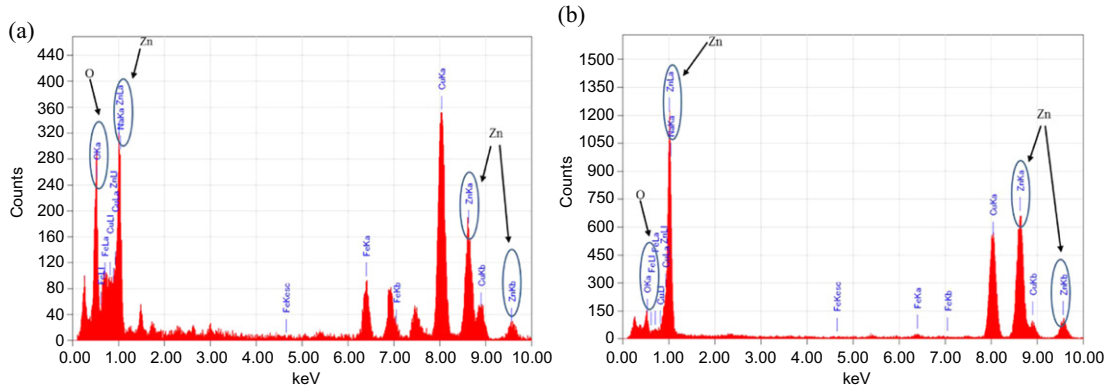

Figure 5. (a) EDS spectra in the dispersion of 0.2 gm ZnO before plasma irradiation. (b) After plasma irradiation.

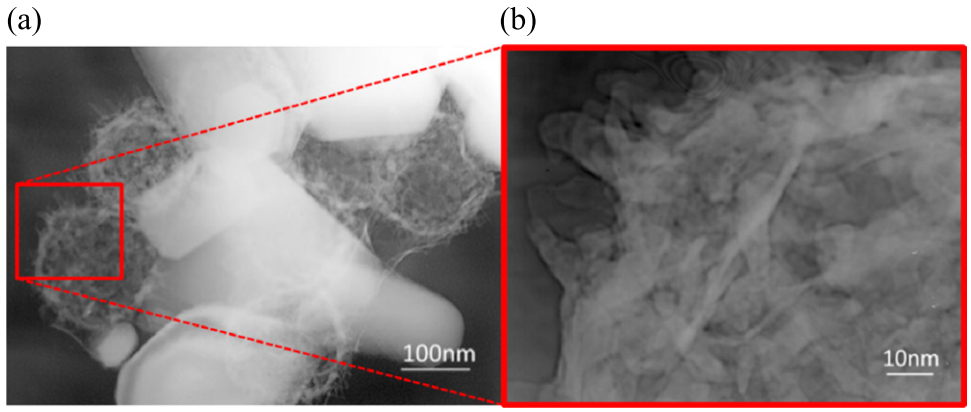

Figure 6. (a) TEM image of nanoparticle in the dispersion of 6.0 gm ZnO in 80 ml ethanol, (b) an enlarged image of a fiber-flocculate spherical particle.

approximately 180 nm. From the enlarged image of the fiber-flocculated spherical particles in figure 6(b), the diameter of one fiber was found to be approximately 10 nm. Figure 7(a) shows the EDS spectrum of the white polygonal particles, sufficient oxygen was detected to determine that the particles consisted of ZnO. On the other hand, according to the EDS spectrum of the fiber-flocculate particles in figure 7(b), hardly any oxygen was present.

Further investigations of the product were performed using x-ray diffraction (XRD). The XRD pattern before and after plasma generations for dispersion of 0.2 g and 6.0 ZnO powder are shown in figures 8(a)–(c), respectively. These spectra were recorded for a whole particle including one that remained in a liquid. Some metallic zinc peaks were observed after plasma generation, although ZnO was dominant.

Under the assumption of reduction due to thermal reaction, the reduction of ZnO is predicted using a consideration of chemical equilibrium and the Ellingham diagram.

The chemical equilibrium can be calculated from chemical potential of all the products. 27 species were given in the calculation as products from ethanol, O, H, H_2, O_2, H_2O, OH, HO_2, H_2O_2, C(g), C_2, C_3, CO, CO_2, C_3O_2, CH, CH_2, CH_3, CH_4, C_2H, C_2H_2, C_2H_4, CH_2O, CH_3OH, HCOOH, CH_2CO, CH_3HCO and C(s). The chemical potential of product p is expressed as follows:

$$\mu_p = \mu_p^0 + RT \ln P_p, \tag{1}$$

Where $\mu_{p\,\mathrm{p}}^0$, R, T, and P_p are the chemical potential of p at standard condition, the gas constant, temperature, and the partial pressure of p, respectively. The μ_p^0 of all the products can be calculated from JANAF thermochemical tables. When all the products are under chemical equilibrium, the chemical potential can be calculated from the three representative chemical potentials such as $\mu_{C\,(s)}$, μ_H, and μ_O as follows:

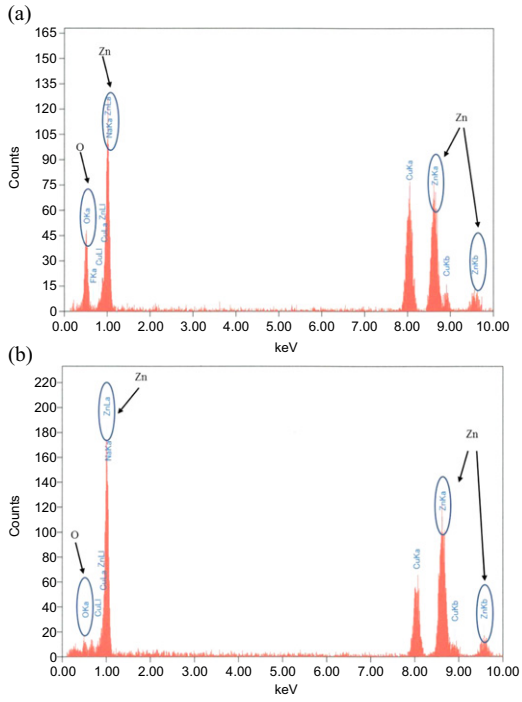

Figure 7. (a) EDS spectra in the dispersion of 6.0 gm ZnO in 80 ml ethanol before plasma irradiation. (b) After plasma irradiation.

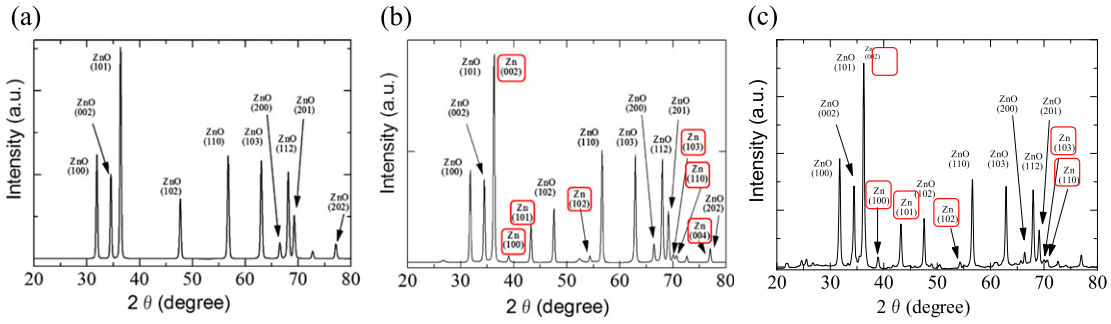

Figure 8. (a) XRD pattern before plasma generation. (b) After plasma irradiation (6.0 g of ZnO). (c) After plama irradiation (0.2 g of ZnO).

$$\mu_p = n_p^{\mathrm{C}}\mu_{C(s)} + n_p^{\mathrm{H}}\mu_{\mathrm{H}} + n_p^{\mathrm{O}}\mu_{\mathrm{O}} \tag{2}$$

where $n_{\mathrm{p}}^{\mathrm{C}}$, $n_{\mathrm{p}}^{\mathrm{H}}$ and $n_{\mathrm{p}}^{\mathrm{O}}$ are the numbers of C, H and O atoms in p, respectively. 24 equations expressed as equation (2) are made up for 24 products except for C(s), H and O. Because there are 27 indeterminate variables, which are chemical potentials, three more equations will be needed to solve them. The atomic ratios of C to H and of O to H have to be retained between the reactants and products expressed as,

$$\sum_p n_p^C \Big/ \sum_p n_p^H = \text{const.} \tag{3}$$

$$\sum_p n_p^O \Big/ \sum_p n_p^H = \text{const.} \tag{4}$$

The total pressure is a determinate value such as 30 kPa, expressed as,

$$\sum_p P_p = \text{const.} \tag{5}$$

If ethanol is used as a solvent, the values of the right side of equations (3) and (4) become 1/3 and 1/6, respectively. Thus, 27 chemical potentials or partial pressures which follow the chemical potentials as expressed in equation (1) can be calculated from equations (2–5).

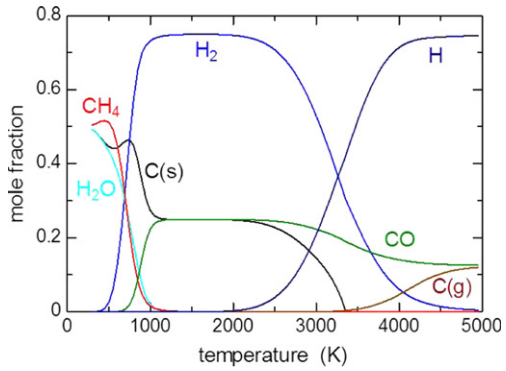

Figure 9. Mole fraction of product.

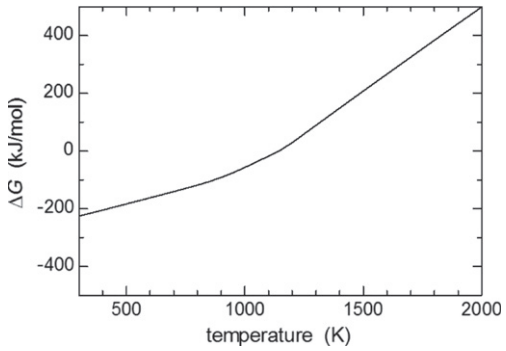

Figure 10. The Gibbs energy change of zinc oxidation.

An Ellingham diagram is used to predict whether the reaction of metals progresses to oxidation or reduction. If a metal oxide of metal M is expressed as M_xO_y, the reaction equation is expressed as follows:

$$\frac{2x}{y}\mathrm{M} + \mathrm{O_2} \leftrightarrow \frac{2}{y}\mathrm{M}_x\mathrm{O}_y \tag{6}$$

The Ellingham diagram shows the Gibbs energy change ΔG^0 by 1 mole O_2 under the partial pressure of O_2 of 1 atm as a function of temperature. The Gibbs energy change ΔG of the reaction changes with the partial pressure of O_2 and is expressed as,

$$\Delta G = \Delta G^0 - RT \ln P_{\mathrm{O2}} \tag{7}$$

The reaction shown in equation (6) progresses from left to right when ΔG is negative, while inversely it progresses from right to left when ΔG is positive. A reducing atmosphere, that is, will be provided when ΔG is positive.

Some mole fractions of dominant products under the chemical equilibrium are shown in figure 9. The maximum mole fraction of O_2 is under 10^{-9}, and is much smaller than the dominant products. The Gibbs energy change of zinc oxidation is shown in figure 10. ΔG increases with the temperature and turns to a positive from a negative at 1140 K. This indicates that if the temperature is higher than 1140 K, the reducing atmosphere is available for zinc oxide.

In-liquid plasma may be suitable for generating a temperature of over 1140 K. It is difficult to measure the temperature, but spectroscopic measurement of plasma emission provides some important information concerning temperature. Line emission spectra of some species can give the excitation temperature through application of the Boltzmann plot method. The excitation temperature is related with the electron temperature. However, the electron temperature is not necessarily the same as the gas temperature, because in-liquid plasma is not necessarily in thermal equilibrium. The excitation temperature of in-liquid plasma is found to be generally between 3000 and 5000 K [31], and decreases with an increase of pressure. When plasma is generated in water, OH spectral band is detected around 310 nm. The rotational temperature of OH radicals can be obtained by matching the configuration of the spectral band to that of computational simulation. The rotational temperature is considered to be close to the gas temperature, because the thermal energy is almost equally

distributed to the translation, rotational and vibrational energy of the molecule. The rotational temperature of in-liquid plasma was found to be generally from 3000 to 5000 K, [31, 32] and increases with the increase of pressure. Finally, the continuous spectrum of the black-body radiation from the electrode can sometimes be detected. By fitting it to the Planck's law, the temperature of the electrode which is in contact with the plasma can be obtained. The temperature of the electrode was found to be roughly between 1300 and 1700 K [32, 33].

All the temperatures shown above exceed 1140 K. Therefore, the reaction field provided by the in-liquid plasma is a reducing atmosphere for zinc oxide.

When the 0.2 gm dispersion of ZnO was used, nearly all the ZnO particles in the dispersion were found to have been converted to Zn particles by the plasma. From this, the energy efficiency can be estimated, knowing that a reduction of 0.2 g (2.5 mmol) ZnO was caused by supplying microwave of 78 kJ to the plasma. From the theoretical enthalpy for reduction of ZnO of 348.3 kJ mol^{-1}, the energy efficiency of the present experiment becomes 1.1%, obtained by the following calculation.

$$\frac{348.3\ \text{kJ mol}^{-1} \cdot 2.5 \times 10^{-3}\ \text{mol}}{235\ \text{W} \cdot 330\ \text{s}(=78\ \text{kJ})} \times 100 = 1.1\% \quad (8)$$

Pyrometallurgy and electrowinning are industrial processes comparable with the present experiment. Both processes require roughly 3000 kWh to 1 ton of metallic zinc, and from these values, the energy efficiency of these processes can be calculated to be 49%.

Another method for zinc recovery that has been reported, the hydrometallurgical method, uses methane and solar thermal technology [34–36] however, these methods have no information regarding the zinc nanoparticle production that is needed for zinc air batteries. This present method provides for recycling of zinc nanoparticles with prevention of re-oxidation, because the reaction area is separated from the air by liquid. An additional advantage to this method is the easy collection of the product since the reduced metal remains in the liquid as dispersed particles.

From the calculation results, two parameters were derived theoretically for the proposed reduction method. One is that the appropriate ratio of ethanol and zinc oxide should be prepared for the plasma, and the other is that the temperature within the plasma should be between 1500 and 2000 K in order to utilize the enthalpy change of ethanol efficiency.

4. Conclusion

Zinc nanoparticles were synthesized from reduction of ZnO powder by 2.45 GHz microwave in ethanol, which act as reducing agents. Nanoparticles in cubic and hexagonal shapes of about 30 to 200 nm along with fiber flocculates 10 nm in diameter were found at the tip of the electrode and in the remaining liquid after plasma generation. This study was conducted simply to confirm the reduction of ZnO by plasma in liquids, and was not intended as an improvement of energy efficiency. In the future, in order to improve the energy efficiency, many parameters must be examined, for example, the type of liquid, frequency, power, pressure, arrangement of the device, and so on. Moreover, the distinctive nanoparticles synthesized by this experiment, and the mechanism of synthesis should be clarified in the future to obtain a more perfect reduction of oxides and synthesize pure metallic zinc nanoparticles.

References

[1] Caramia M and Bozzini B 2014 *Mater. Renew. Sustain. Energy* **3** 28
[2] Bergman M 2013 *Master Thesis,* Division of Condensed Matter Physics, Chalmers University of Technology
[3] Wen Y-H, Cheng J, Ning S-Q and Yang Y-S 2009 *J. Power Sources* **188** 301
[4] Lee J-S, Kim S T, Cao R, Choi N-S, Liu M, Lee K T and Cho J 2011 *Adv. Energy Mater.* **1** 34
[5] Moon E, Kim J, Nam S and Eom S 2012 *Japan. J. Appl. Phys.* **02** 51
[6] Lee S-H, Jeong Y-J, Lim S-H, Lee E-A, Yi C-W and Kim K 2010 *J. Korean Electrochem. Soc.* **13** 45
[7] Xu Y, Xu X, Li G, Zhang Z, Hu G and Zheng Y 2013 *Electrochem. Sci.* **8** 11805
[8] Kraytsberg A and Ein-Eli Y 2013 *Nano Energy* **2** 468
[9] Hattori Y, Mukasa S, Toyota H, Inoue T and Nomura S 2011 *Mater. Lett.* **65** 188
[10] Vaghayenegar M, Kermanpur A, Abbasi M H and Yazdabadi H G 2010 *Adv. Powder Tech.* **21** 556
[11] Purohit V S, Ded S, Bhattacharya S K, Kshirsagar A, Dharmadhikari C V and Bhoraskar S V 2008 *Nucl. Instrum. Methods Phys. Res.* B **266** 4980
[12] Peng X S, Zhang L D, Meng G W, Yuan X Y, Lin Y and Tian Y T 2003 *J. Phys. D: Appl. Phys.* **36** L35
[13] Li J and Chen X 2004 *Solid State Commun.* **131** 769
[14] Zhu Y C and Bando Y 2003 *Chem. Phys. Lett.* **372** 640
[15] Hattori A N, Ichimiya M, Ashida M and Tanaka H 2012 *Appl. Phys. Express* **5** 125203
[16] Fujisawa H, Kuri R, Shimizu M, Kotaka Y and Honda K 2009 *Appl. Phys. Express* **2** 055003
[17] Jun I, Sunwoo N, Sung L, Kim H, Woo J and Shin C P 2013 *Japan. J. Appl. Phys.* **52** 025003
[18] Kawakami M, Hartanto A B, Nakata Y and Okada T 2003 *Japan. J. Appl. Phys.* **42** L33

[19] Kitamura K, Yatsui T and Ohtsu M 2008 *Appl. Phys. Express* **1** 081202
[20] Oh S, Nagata T, Volk J and Wakayama Y 2012 *Appl. Phys. Express* **5** 095003
[21] Park S, Jung W and Park C 2013 *Japan. J. Appl. Phys.* **52** 025502
[22] Int. Zinc Association, Zinc Recycling 2011 *Closing the Loop* www.zinc.org
[23] Hattori Y, Mukasa S, Toyota H, Inoue T and Nomura S 2011 *Mater. Chem. Phys.* **131** 425
[24] Hattori Y, Nomura S, Mukasa S, Toyota H, Inoue T and Kasahara T 2013 *J. Alloys Compd.* **560** 105
[25] Hattori Y, Nomura S, Mukasa S, Toyota H, Inoue T and Kasahara T 2013 *J. Alloys Compd.* **560** 105
[26] Kubo S and Nakagawa M 2012 *Chem. Lett.* **41** 1137
[27] Singh S C, Swarnkar R K and Gopal R 2010 *Bull. Mater. Sci.* **33** 21–6
[28] Khoza P B, Moloto M J and Sikhwivhilu L M 2012 *J. Nanotechnol.* **2012** 1
[29] Singh S C and Gopal R 2007 *Bull. Mater. Sci.* **30** 291
[30] Revina A A, Oksentyuk E V and Fenin A A 2007 *Protection of Metals* **43** 554
[31] Nomura S, Mukasa S, Toyota H, Miyake H, Yamashita H, Maehara T, Kawashima A and Abe F 2011 *Plasma Source Sci. Technol.* **20** 034012
[32] Maehara T *et al* 2008 *Plasma Chem. Plasma Process* **28** 467–82
[33] Nomura A, Toyota H, Mukasa S, Takahashi Y, Maehara T, Kawashima A and Yamashita H 2008 *Appl. Phys. Express* **1** 046002
[34] Liao J, Wu H, Fu W, Ci S and Chen Q 2012 *Hydrometallurgy* **121–124** 107–15
[35] Ebrahim H and Jamshidi E 2001 *Trans. Chem.* E **79** 62–70
[36] Wieckert C and Steinfield A 2002 *J. Solar Energy Eng.* **124** 55–62